Manuscript title: *Thermodynamic modelling of the statistics of cell spreading on ligand coated elastic substrates*

Running title: *A thermodynamic model of cell spreading*

Eoin McEvoy, Siamak S. Shishvan, Vikram S. Deshpande, J. Patrick McGarry

Abstract

Biological spread cells exist in a perpetually fluctuating state, and therefore cannot be described in terms of a unique deterministic system. In order for modelling approaches to provide novel insight and uncover new mechanisms that drive cell behaviour, a framework is required that progresses from traditional deterministic methods (whereby simulation of an experiment predicts a single outcome). In this study we implement a new modelling approach for the analysis of cell spreading on ligand coated substrates, extending the framework for non-equilibrium thermodynamics of cells developed by Shishvan *et al.* (2018) to include active focal adhesion assembly. We demonstrate that the model correctly predicts the coupled influence of surface collagen density and substrate stiffness on cell spreading, as reported experimentally by Engler *et al.* (2003). Low surface collagen densities are shown to result in a high probability that cells will be restricted to low spread areas. Furthermore, elastic free-energy induced by substrate deformation lowers the probability of observing a highly spread cell, and consequentially lower cell tractions affect the assembly of focal adhesions. Experimentally measurable observables such as cell spread area and aspect ratio can be directly post-processed from the computed homeostatic ensemble of (several million) spread states. This allows for the prediction of mean and standard deviations of such experimental observables. This class of cell mechanics modelling presents a significant advance on conventional deterministic approaches.

Keywords: Statistical mechanics, Cell spreading, Focal adhesion assembly, Homeostatic ensemble

1. Introduction

There is no unique outcome for tissue development in nature. For example, examination of arterial tissue across several samples reveals non-homogenous structures with non-uniform collagen fibre alignment, tissue thickness, and smooth muscle cell (SMC) morphology (1–3). The same is true *in-vitro*, where cells of the same phenotype exhibit a diverse range of spread shapes, area, stress-fibre alignments, and focal adhesion distributions. However, over large populations the statistics of observables is highly reproducible. Several experimental studies have demonstrated that the microenvironment has a significant impact on cell behavior. Jacot *et al.* (4) show that sarcomere development and alignment in cardiomyocytes are dependent on substrate stiffness. A study by Arnold *et al*. (5) reveals that focal adhesion (FA) and stress-fibre (SF) formation are limited by ligand spacing on the substrate. Engler *et al*. (3) show that both the mean and standard error of SMC spread area depend on substrate rigidity and ligand density: with decreasing surface collagen density and decreasing substrate stiffness, the standard error reported for the experiment reduces.

It is therefore evident that in order to uncover the biomechanisms underlying such observations, a statistical mechanics approach to cell modelling is required. Typically, previous models have assumed the spread state as the reference configuration and simulate a single deterministic outcome (6–12). McEvoy *et al*. (13) recently implemented a framework whereby an initially unadhered cell deforms to a range of possible spread states, and the system free-energy is computed for each configuration. It is demonstrated that cell spreading entails a competition between the increasing elastic free-energy due to stretching of passive cell components, and the decreasing cytoskeletal free-energy as contractile proteins assemble to form stress-fibres. Such a competition allows for the identification of a low free-energy state, and it is shown that the predicted cell areas and SF alignments in these configurations are similar to reported experimental measurements (14). However, in the study of McEvoy *et al.* (13) a single low energy spread state is identified. This deterministic approach neglects the fact that cells display a fluctuating response to their microenvironment in terms of observables such as SF alignment and spread area.

In this study, we implement a statistical mechanics framework for the *homeostatic ensemble of spread cells*, following the approach of Shishvan *et al.* (15). This methodology allows for the simulation of a large collection of spread microstates the cell-substrate system assumes while maintaining its homeostatic state. The framework incorporates mathematical models to describe SF formation and cell-substrate deformation. Here we expand the model for calculation of Gibbs free-energy to include the free-energy associated with the traction dependent focal adhesion (FA) assembly. Simulations accurately predict the dependence of cell area and shape on surface collagen density and substrate stiffness, as reported in the experimental study of Engler *et al.* (3).

2. Methodology

We aim to analyse the response of cells adhered to collagen coated elastic substrates. This experimental system is responding to both mechanical and chemical cues from its environment, viz. the stiffness of the substrate and the extra-cellular proteins (collagen) through which the cells adhere to the substrates. The response of this complex system is recorded through a range of observables, all of which exhibit large variations but with trends clearly emerging when the statistics of these observables are analysed. This motivates our choice of a modelling framework, called homeostatic statistical mechanics (15), in which, just as in the experimental system, observables fluctuate while trends (and understanding) emerge once these observables are viewed statistically. This framework has previously been shown to successfully capture a range of observations for smooth muscle cells (SMCs) seeded on elastic substrates in which perfect adhesion was assumed and the role of the extra-cellular matrix neglected. Here we extend the framework to include an adhesion model and thus will first give a brief overview of the modelling framework (details in **Supplementary Information Section 1**) and then focus on the adhesion model.

2.1. Overview of the homeostatic mechanics framework

The homeostatic mechanics framework recognises that the cell is an open system which exchanges nutrients with the surrounding nutrient bath. These high-energy nutrient exchanges fuel fluctuations in cell responses associated with various intracellular biochemical processes (such non-thermal nutrient-fuelled fluctuations are observed to be very large and occur over very long time-scales, compared to conventional thermal fluctuations). However, these biochemical processes attempt to maintain the cell in a homeostatic state, i.e. the cell actively maintains its various molecular species at a specific average number over these fluctuations that is independent of the environment. This translates to the constraint on the average Gibbs free-energy (16) of the cell. Employing the *ansatz* that biochemical processes such as actin polymerisation and treadmilling provide the mechanisms to maximise the morphological entropy of the cell subject to the constraint that the cell maintains a homeostatic state, Shishvan *et al.* (15) obtained the distribution of states that the cell assumes in terms of the Gibbs free-energy $G^{(j)}$ of morphological state (j) of the system as

$$P_{\mathrm{eq}}^{(j)} = \frac{1}{Z}\exp\left(-\zeta G^{(j)}\right). \tag{1}$$

$Z \equiv \sum_j \exp\left(-\zeta G^{(j)}\right)$ is the partition function of the morphological microstates, and the distribution parameter ζ follows from the homeostatic constraint

$$\frac{1}{Z}\sum_j G^{(j)} \exp\left(-\zeta G^{(j)}\right) = G_{\mathrm{S}}\,, \tag{2}$$

where G_{S} is equal to the equilibrium Gibbs free-energy of an isolated cell in suspension (free-standing cell), i.e. the homeostatic processes maintain the average biochemical state of the system equal to that of a cell in suspension. Thus, the distribution (eq. (1)) is characterised by a homeostatic temperature $1/\zeta$ that is conjugated to the morphological entropy of the cell. We employ Markov Chain Monte Carlo (MCMC) to construct a Markov chain that is representative of the homeostatic ensemble. This involves three steps: (i) a discretisation scheme to represent morphological microstate (j), (ii) calculation of $G^{(j)}$ for a given morphological microstate (j), and (iii) construction of a Markov chain comprising these morphological microstates. Typical Markov chains comprised in excess of 2.5 million spread states (a detailed overview of the procedure is provided in **Supplementary Information Section 2.2**).

2.2 Free-energy $G^{(j)}$ of a morphological state

Much like conventional statistical mechanics frameworks that require a model for the energy of molecular systems, the homeostatic statistical mechanics framework requires a model for the Gibbs free-energy $G^{(j)}$ of a morphological state (j) of the system. Here, we employ a relatively simple model for the Gibbs free-energy wherein the cell consists of a passive elastic nucleus within a cytoplasm that is modelled as comprising an active stress-fibre cytoskeleton and elements such as the cell membrane, intermediate filaments and microtubules that are all lumped into a single passive elastic contribution.

Details of the model including the parameters used to characterise the SMCs are given in **Supplementary Information Section 2.** Here we briefly describe the salient features of the model for SMCs on elastic substrates. The SMCs are modelled as two-dimensional (2D) bodies in the $x_1 - x_2$ plane lying on the surface of an elastic substrate such that the out-of-plane Cauchy stress $\Sigma_{33} = 0$. The substrates are modelled as linear elastic half-spaces while the cells are modelled using the approach of Vigliotti *et al.* (17) as modified by Shishvan *et al.* (15). The Vigliotti *et al.* (17) model assumes only two elements within the cell: (i) a passive elastic contribution from elements such as the cell membrane, intermediate filaments and microtubules and (ii) contractile acto-myosin stress-fibres that are modelled explicitly. The cell in its undeformed state is a circle of radius R_0 and for a given morphological microstate (j), the strain distribution within the cell is specified. This directly gives the elastic strain energy of the cell $\hat{F}_{\text{passive}}$ via a 2D Ogden-type hyperelastic model for both the nucleus and cytoplasm. The passive hyperelastic behaviour of the cytoplasm and nucleus has been characterised for several cell types using experimental techniques in which stress fibres are disrupted using cyto-D (18–20). The stress-fibre cytoskeleton within the cytoplasm is modelled as a distribution of stress-fibres such that at each location x_i within the cell $\hat{\eta}(\varphi)$ parameterises the angular concentration of stress-fibres over all angles φ, while $\hat{n}^{ss}(\varphi)$ denotes the number of functional units within each stress-fibre. Thus, at any x_i there is a total concentration $\hat{N}_{\text{b}}$ of bound stress-fibre proteins obtained by integrating $\hat{\eta}\hat{n}^{ss}$ over all orientations φ and these bound proteins are in chemical equilibrium with the unbound stress-fibre proteins. The unbound proteins are free to diffuse within the cell and thus at equilibrium of a morphological microstate the concentration $\hat{N}_{\mathrm{u}}$ of these unbound stress-fibre proteins is spatially uniform. This chemical equilibrium condition along with the conservation of stress-fibre proteins within the cell provides the spatial and angular distributions of stress-fibres from which the free-energy of the cytoskeleton $\hat{F}_{\mathrm{cyto}}$ is evaluated. The total normalised free-energy of the cell morphological microstate (j) then follows as $\hat{G}^{(j)} \equiv \hat{F}^{(j)}_{\mathrm{passive}} + \hat{F}^{(j)}_{\mathrm{cyto}} + \hat{F}^{(j)}_{\mathrm{sub}}$, where $\hat{F}^{(j)}_{\mathrm{sub}}$ is the elastic energy of the substrate ($\hat{G}^{(j)}$ is the normalised value of $G^{(j)}$; see **Supplementary Information Section 2.4** for details of the normalisations).

In addition to the contributions to $\hat{G}^{(j)}$ from the passive elasticity and cytoskeleton of the cell, here we also include the contribution from the focal adhesions between the cell and the collagen extra-cellular matrix (ECM) laid on the elastic substrates on which the SMCs are seeded. Shishvan *et al.* (15) implicitly assumed an unlimited supply of adhesion proteins as well as extra-cellular proteins to form adhesion complexes and thereby neglected the contribution of adhesion to $\hat{G}^{(j)}$. Here we extend the approach of Shishvan *et al.* (15) for the case of a finite quantity of both focal adhesion proteins and extra-cellular collagen and thus explicitly include an adhesion contribution to $\hat{G}^{(j)}$, i.e. we write $\hat{G}^{(j)}$ as

$$\hat{G}^{(j)} \equiv \hat{F}^{(j)}_{\mathrm{passive}} + \hat{F}^{(j)}_{\mathrm{cyto}} + \hat{F}^{(j)}_{\mathrm{sub}} + \hat{F}^{(j)}_{\mathrm{adh}}. \tag{3}$$

We now proceed to make explicit this adhesion model.

2.3 Adhesion complexes between the cell and the extra-cellular collagen

The focal adhesion model proposed here is a modification to the model of McEvoy *et al.* (13) where adhesion is assumed to be via integrins that exist in a single state. These integrins form complexes by binding to ligands that have a density N_{H} per unit area on the surface of the elastic substrate. For a given morphological microstate (j), the strain state of the cell is specified and this implies that the tractions $\mathrm{T}_i(x_i)$ the cells exert on the substrate are also fixed from the cell model; see **Supplementary Information Section 2.1** (for the sake of brevity here we have dropped the superscript (j) to indicate that these are tractions for a given morphological microstate (j)). These tractions are transmitted to the substrate through the focal adhesion complexes and here we explain the adhesion model with the tractions $\mathrm{T}_i(x_i)$ specified.

When in local equilibrium at a location x_i on the surface of the cell, the integrins with a local concentration $C_\mathrm{I}(x_i)$ have a chemical potential at temperature T in terms of the Boltzmann constant k_B

$$\chi_\mathrm{I}(x_i) = \mu_\mathrm{I}(x_i) + k_\mathrm{B}T\ln\left(\frac{\bar{C}(x_i)}{1-\bar{C}(x_i)}\right), \tag{4}$$

where μ_I is their enthalpy while $\bar{C}(x_i) \equiv C_\mathrm{I}(x_i)/C_\mathrm{r}$, in terms of the number of integrin sites per unit area C_r on the cell membrane. The enthalpy of the integrins follows from recalling that each integrin molecule transmits a force $\text{Ƒ}(x_i)$ related to the traction $\mathrm{T}(x_i) \equiv \sqrt{\mathrm{T}_1(x_i)^2 + \mathrm{T}_2(x_i)^2}$ on the cell surface via $\mathrm{T}(x_i) = \text{Ƒ}(x_i)N_\mathrm{H}$. Then,

$$\mu_\mathrm{I}(x_i) = \Phi\big(\Delta(x_i)\big) - \text{Ƒ}(x_i)\Delta(x_i), \tag{5}$$

where Δ is the stretch of the focal adhesion complex and Φ the internal energy of the complex subjected to a stretch Δ. Now assuming linear behaviour of the complex with a stiffness κ_s, such that $\text{Ƒ}(x_i) \equiv \kappa_\mathrm{s}\,\Delta(x_i)$, eq. (5) reduces to $\mu_\mathrm{I}(x_i\ ) = -\text{Ƒ}(x_i)^2/2\kappa_\mathrm{s}$ and the chemical potential follows as

$$\chi_\mathrm{I}(x_i) = k_\mathrm{B}T\ln\left(\frac{\bar{C}(x_i)}{1-\bar{C}(x_i)}\right) - \frac{\text{Ƒ}(x_i)^2}{2\kappa_\mathrm{s}}. \tag{6}$$

The integrins are mobile over the surface membrane and at equilibrium, their chemical potentials are spatially uniform such that $\chi_\mathrm{I}(x_i) = \chi_\mathrm{C}$. The equilibrium concentrations $\bar{C}_\mathrm{eq}(x_i)$ then follow in terms of χ_C as

$$\left(\frac{\bar{C}_\mathrm{eq}(x_i)}{1-\bar{C}_\mathrm{eq}(x_i)}\right) = \exp\left(\frac{\chi_\mathrm{C} + \frac{\text{Ƒ}(x_i)^2}{2\kappa_\mathrm{s}}}{k_\mathrm{B}T}\right). \tag{7}$$

However, χ_C is as yet unknown and the conservation of integrins provides the additional constraint to determine χ_C, viz. given a spatially uniform surface density C_0 of integrins for a cell in suspension, the conservation statement reads

$$A_0C_0 = C_\mathrm{r}\int_A \bar{C}_\mathrm{eq}(x_i)dA, \tag{8}$$

where A_0 is the surface area of the cell in suspension and A its area in the current configuration. The simultaneous solution of eq. (7) and eq. (8) gives χ_C and the adhesion free-energy of the cell is then given as $F_\mathrm{adh} = A_0C_0\chi_\mathrm{C}$.

The above analysis assumes the adhesion complexes can sustain any required force $\mathcal{F}(x_i)$ via the assumed linearity of the complex response. However, it has been demonstrated that complexes cannot support a force greater than a critical value $\mathcal{F}_{\mathrm{max}}$ (21–23). Direct enforcement of the condition that no complex force exceeds $\mathcal{F}_{\mathrm{max}}$ at the cell-substrate interface would require an iterative adjustment of spread state (as implemented for simplified microstates by McEvoy et al. (13)), and is therefore excessively computationally expensive in the context of the Monte Carlo simulations required for sampling the homeostatic ensemble. Here we use the alternative approach of a penalty scheme to ensure that a very small number of spread states contain complexes with forces $\mathcal{F} > \mathcal{F}_{\mathrm{max}}$. In summary, we define a penalty force

$$\mathcal{F}^{\mathrm{p}} = \int_A \Delta\mathcal{F}^{\mathrm{p}}(x_i)\, dA, \tag{9}$$

where

$$\Delta\mathcal{F}^{\mathrm{p}}(x_i) = \begin{cases} \mathcal{F}(x_i) - \mathcal{F}_{\mathrm{max}} & \mathcal{F}(x_i) > \mathcal{F}_{\mathrm{max}} \\ 0 & \text{otherwise.} \end{cases} \tag{10}$$

A penalty energy is then defined as $\chi_{\mathrm{p}} = (\mathcal{F}^{\mathrm{p}})^2/(2\kappa_{\mathrm{p}})$, where the parameter κ_{p} has the units of stiffness and sets the magnitude of the penalty. The total focal adhesion free-energy including the penalty contribution is then defined as

$$F_{\mathrm{adh}} = A_0 C_0 (\chi_{\mathrm{C}} + \chi_{\mathrm{p}}), \tag{11}$$

with the normalised energy $\hat{F}_{\mathrm{adh}}$ following from the definitions detailed in **Supplementary Information Section 2.4** along with the model parameters. In order to compare model predictions with the experimental results of Engler *et al.* (3), the number of ligands per unit area, N_{H}, can be expressed as surface collagen density ρ_{col} through the following expression:

$$\rho_{\mathrm{col}} = N_{\mathrm{H}} M_{\mathrm{col}}/L \ , \tag{12}$$

where M_{col} is the molar mass of collagen and L is Avogadro's constant. We assume a uniform surface collagen distribution and substrate stiffness.

3. Results and Discussion

3.1. Spread dependence of cells on surface collagen density

The influence of surface collagen density ρ_{col} on cell spreading is shown in Figure 1. Cells are spread on rigid substrates coated with three different values of ρ_{col} (6, 33, and 250 $\mathrm{ng\,cm^{-2}}$). A sample of cell spread states, with the same free-energy for a given ρ_{col}, are shown in Figure 1a, including stress fibre distributions (green), focal adhesion distributions (red), and nuclei (blue). In the case of a low ρ_{col} (i.e. 6 $\mathrm{ng\,cm^{-2}}$) cells are not highly spread and they maintain regular rounded morphologies. A low concentration smeared actin cytoskeleton is observed throughout the cell, with no regions of highly aligned stress fibres. For a higher ρ_{col} of 33 $\mathrm{ng\,cm^{-2}}$, cells become more highly spread. Additionally, the spread shapes become quite irregular, in contrast to the rounded shapes observed on a lower ρ_{col}. Regions of aligned stress fibres are observed and focal adhesions cluster towards the cell periphery. In the case of the highest ρ_{col} of 250 $\mathrm{ng\,cm^{-2}}$, a further increase in spread area is observed and the spread shape becomes highly irregular, with cells exhibiting elongated protrusions. High concentrations of aligned stress fibres are observed, and focal adhesions are highly localised at the cell periphery and cell nucleus.

Probability density functions (pdfs) for cell spread area (Figure 1b) and for cell aspect ratio (AR) of a best fit ellipse (Figure 1c) are constructed from the full population of spread states for each surface collagen density. With increasing ρ_{col}, the mean cell spread area increases and the variance in spread area increases (i.e. in Figure 1a, as ρ_{col} increases the pdf moves to the right and becomes less peaked). A similar trend is observed for cell aspect ratio (Figure 1c), where the mean is closer to 1 and the variance is very low (the pdf is more peaked) for the lowest ρ_{col}. In summary, the pdfs presented in Figures 1b and 1c show that a population of cells on a lower ρ_{col} will have a lower mean spread area and a lower variance of spread area, in addition to being rounded (AR close to 1) with a low variance of spread shape. As ρ_{col} increases, a higher mean spread area is obtained for a population of cells, with a higher variance of spread area and spread shape. Additional spread shapes are presented in Supplementary Data Figures SI-1 and SI-2.

3.2. Influence of substrate stiffness on cell spreading

The influence of substrate stiffness E_{sub} on cell spreading is shown in Figure 2. Cells are spread on substrates of stiffness 8 kPa and 32 kPa, in addition to a rigid substrate. All substrates have a ρ_{col} of 33 $\mathrm{ng\,cm^{-2}}$. A sample of cell spread states shown in Figure 2a suggests that cell spread area increases with E_{sub}. Cells on the compliant (8 kPa) substrate exhibit a low concentration smeared actin cytoskeleton, compared to the highly aligned stress fibres on the stiff and rigid substrate. The irregularity of the spread shape increases with E_{sub}, with longest protrusions occurring on the rigid substrate.

Probability density functions for cell spread area (Figure 2b) and aspect ratio (Figure 2c) are constructed from the full population of spread states for each value of E_{sub}. Clearly both the mean spread area and the variance in spread area increase with E_{sub} (i.e. in Figure 2b the pdf moves to the right and becomes less peaked as E_{sub} is increased). The effect of E_{sub} on cell shape is less pronounced for the value of ρ_{col} considered here, with only a minor increase in the mean and variance of cell aspect ratio with increasing stiffness (Figure 2c).

3.3. Coupled dependence of collagen density and substrate stiffness

The coupled interplay between the influence of ρ_{col} and E_{sub} on cell spreading is next considered. Contour plots are constructed from mean spread areas (Figure 3a) and mean aspect ratios (Figure 3b). Representative spread states are superimposed for illustrative purposes. As shown in Figure 3a, a very low ρ_{col} results in a very weak dependence of mean spread area on E_{sub}. However, for moderate and high ρ_{col} the mean spread area is highly dependent on E_{sub}. As shown in Figure 3b, the cell aspect ratio exhibits a very weak dependence on E_{sub} (the contours in 4b are almost uniform in the vertical direction), while exhibiting a very strong dependence on ρ_{col}.

Both the mean and standard deviation of cell spread area is shown in Figure 3c. A number of features should be noted: (i) as ρ_{col} is increased, both the mean and standard deviation increase up to a peak value. This trend is observed for all values of E_{sub}; (ii) if ρ_{col} is increased beyond the peak value, a slight reduction in mean spread area (and its standard deviation) is observed. Again, this trend is observed for all values of E_{sub}; (iii) the ρ_{col} at which the mean spread area reaches a peak value increases with increasing E_{sub}; (iv) for a given ρ_{col}, both the mean and standard deviation increase with increasing E_{sub}. Figure 3d shows that cell aspect ratio is highly dependent on ρ_{col}, with both the mean and standard deviation increasing with increasing ρ_{col}. It is interesting to note that even though the cell mean spread area decreases when the ρ_{col} is increased beyond the critical value, the mean aspect ratio continues to increase. However, mean aspect ratio and its standard deviation exhibits a weak dependence on E_{sub}.

3.4. Experimental support for predicted cell behaviour

Remarkably, all the features described by Figure 3 are directly supported by the experimental study of Engler *et al.* (3), where the response of smooth muscle cells (SMCs) to E_{sub} and ρ_{col} was investigated. At a low ρ_{col} on all substrates, SMCs that were detectably spread were found to be rounded with a low spread area. As the ρ_{col} was increased, the spread area (mean and standard deviation) was observed to increase up to a peak value. Following this peak, any increase to the density of ρ_{col} resulted in a reduction of mean spread area. This behaviour is further supported by the experimental study of Gaudet *et al.* (24). Engler *et al.* (3) noted that the ρ_{col} at which the peak mean spread area occurs is dependent on E_{sub}, i.e. it increases with increasing E_{sub}, as predicted by our models). They also reported that an increase in E_{sub} results in a higher mean cell spread area for a fixed ρ_{col}.

Although the aspect ratio is not directly measured in the experimental work of Engler *et al.* (3), with an increase in cell area (due to E_{sub} or ρ_{col}) it was reported that cell shapes became less rounded and more irregular when cell spread area increases as a result of increased E_{sub} and/or ρ_{col}. Such a reduction in cell roundness with increasing E_{sub} has also been observed in the experimental study of Ren *et al.* (25) for skeletal muscle cells. Additionally, Prager-Khoutorsky *et al.* (26) reported that cells readily elongate (i.e. high aspect ratio) when plated on rigid substrates, with the behaviour significantly less pronounced with decreasing E_{sub}. Similar to our predictions for stress fibre distributions, Engler *et al.* (3) report that highly spread cells display a well-ordered stress-fibre network. Such ordered fibres were far less probable on rounded cells on low ρ_{col} and on softer substrates. Similar observations are also reported in the experimental study by Deroanne *et al.* (27) in which a significant reduction in stress fibre and focal adhesions formation was observed in endothelial cells on soft gels compared to stiff substrates. Pelham and Wang (28) also showed such dependence of adhesion formation on substrate stiffness. The predicted trends of SF and FA organisation in Figures 1 and 2 of the current study are strongly supported by the aforementioned experimental studies. Additional samples of computed cell spread states are shown in Supplementary Data Figures SI-1 and SI-2.

3.5. Thermodynamically motivated insights and explanations for predicted cell behaviour

We next provide a thermodynamically motivated explanation for the computed results in Figures 1-3, and, by extension, for the experimental observations of Engler *et al.* (3). In Figure 4a we plot the pdf of Gibbs free-energy for the three values of ρ_{col} on a rigid substrate. Recall that the system is subject to the homeostatic constraint, such that the mean Gibbs free-energy of all states is equal to the cellular homeostatic free-energy G_{S}, which can be identified from the unique state of a free-standing cell. Therefore, the mean free-energy is similar for all values of ρ_{col} (Figure 4a). The pdf for adhesion free-energy (Figure 4b) is highly peaked and negative for a high ρ_{col} of 250 $\mathrm{ng\,cm^{-2}}$. This indicates a high probability that adhesion complex forces are close to $\digamma_{\mathrm{max}}$ so that a low adhesion energy is obtained. On the other hand, there is a low probability that adhesion complex forces exceed $\digamma_{\mathrm{max}}$ and incur a (positive) adhesion energy penalty.

In the case of a high ρ_{col} of 250 $\mathrm{ng\,cm^{-2}}$, the cell-substrate tractions for a wide range of highly spread states can be supported without incurring an adhesion energy penalty (i.e. the adhesion free-energy remains low). As a result the entropy of spread states is very high for high values of ρ_{col}. Correspondingly, a high variance in the (negative) cytoskeletal and (positive) elastic free energies (Figures 4c, d) occurs. In effect, cell spreading on a rigid substrate coated with a high ρ_{col} can be viewed as a competition between positive elastic free-energy due to stretching of passive cell components and negative free-energy due to assembly of contractile stress fibres, with an additional negative free-energy contribution from the adhesion complexes.

When ρ_{col} is reduced, higher forces occur in ligand complexes, resulting in a higher probability that $\digamma_{\mathrm{max}}$ is exceeded and an adhesion energy penalty is incurred. Therefore, there is a low probability that highly spread states will occur, and the entropy of spread states decreases. In other words, a highly spread cell on a low ρ_{col} will result in adhesion complex forces that exceed the maximum value, and the imposition of an energetic penalty results in a low probability that such highly spread states will occur. This explains the high probability of rounded cells with low spread areas on a ρ_{col} of 6 $\mathrm{ng\,cm^{-2}}$, as reported in Figures 1 and 3.

Correspondingly, as shown in Figures 4c and 4d, the cytoskeletal and elastic free-energy pdfs are highly peaked with mean values close to zero (as expected for the observed low spread areas and low variance in spread shapes (AR)).

Recall from Figure 3 that, for all values of E_{sub}, cell spread area increases with increasing ρ_{col} up to a peak value. In Figure 5, we report the mean and standard deviation of the free-energy densities across all ρ_{col} and E_{sub} (the standard deviation is indicative of the variance observed in the corresponding pdfs). The peak spread areas shown in Figure 3b coincide with the lowest mean adhesion free-energy for each substrate (Figures 5(a-c)). The ρ_{col} associated with such a peak spread area on each substrate is hereafter referred to as "optimal". At this optimal ρ_{col} there is a high probability that the forces in adhesion complexes will result in a low adhesion free-energy. For sub-optimal ρ_{col}, highly spread states will result in an increased probability of adhesion complex forces higher than $\mathfrak{F}_{\mathrm{max}}$, resulting in an energetic penalty, as explained in Figure 4 above. On the other hand, when the ρ_{col} is increased beyond the "optimal" value, the cell must spread to a higher area in order to generate sufficient tractions to achieve sufficiently high adhesion complex forces (i.e. $\mathfrak{F}(x_i) \cong \mathfrak{F}_{\mathrm{max}}$) and a low adhesion free-energy. However, spreading to such a high area results in an increased elastic strain energy. There is a low probability that the adhesion (Figure 5 (a-c)) and cytoskeletal (Figure 5 (d-f)) free-energy will overcome this "elastic penalty" and achieve the homeostatic state, i.e. $\hat{G}_{\mathrm{S}}$. Therefore, on "post-optimal" ρ_{col} there is a low probability that the cell area will increase beyond the peak spread area. In fact, a "post-optimal" ρ_{col} leads to a reduction in mean spread area, as shown in Figure 3c (this has been also observed experimentally by Engler *et al.* (3) and Gaudet *et al.* (24), as discussed in Section 3.4 above). This occurs because cellular tractions are supported by a higher number of complexes, so that individual bond forces are reduced. Therefore, the cell adhesion free-energy moves towards zero (Figure 5(a-c)), providing a weaker competition to the elastic strain energy (Figures 5 (g-i)) so that there is a lower probability that the cell will achieve the peak spread area. Although the mean spread area decreases for "post-optimal" ρ_{col}, the mean elastic free-energy increases on rigid and stiff substrates (Figure 5g-h). This is due to a high variability in spread shape on stiffer substrates with high ρ_{col} (see plots of cell aspect ratio in Figure 3d).

A reduction in E_{sub} lowers the probability of the cell achieving a high spread area, with rounded low spread morphologies more frequently observed (Figure 3c). On a rigid substrate, there is no contribution from the elastic strain energy of the substrate (Figure 5j) as it is not deformed by the contractile activity of the cell. However, as the E_{sub} is reduced (Figures 5 k,l), it will be deformed by the cell. The associated substrate free-energy causes the total system free-energy to become increasingly positive. Thus, to achieve a homeostatic state, there is a high probability that the cell area will be lower on more compliant substrates. The highly coupled balance between the contributions to the system free-energy causes the peak cell area to occur at a lower ρ_{col} for a lower E_{sub}. As mentioned above, a low E_{sub} results in lower spread areas, which leads to lower cell-substrate tractions. Therefore, a lower ρ_{col} is required for an increased probability of optimal forces in adhesion complexes ($Ƒ(x_i) \cong Ƒ_{\mathrm{max}}$) and a correspondingly low adhesion free-energy. Peak spreading occurs on lower ρ_{col} for lower E_{sub}, as shown in Figure 3c (and as reported in the experimental of Engler *et al.* (3)).

4. Concluding Remarks

The equilibrium statistical mechanics framework developed by Shishvan *et al.* (15) allows for the simulation of the homeostatic ensemble for cells on an elastic substrate in a nutrient bath. Cells assume a dynamic homeostatic equilibrium by means of a free-energy competition between the increasing elastic free-energy due to stretching of passive cell components (and substrate deformation), and the decreasing cytoskeletal free-energy as contractile proteins assemble to form stress-fibres. In the current study, the framework is expanded to include the free-energy associated with formation of focal adhesions between the cell and a collagen coated substrate.

The expanded framework allows for the simulation of the coupled influence of surface collagen density ρ_{col} and substrate stiffness E_{sub} on cell spreading, as reported in the experimental study of Engler *et al.* (3). The key experimental observations predicted by our modelling framework are summarized as follows:

- With increasing substrate ρ_{col}, cell spread area (mean and standard deviation) increases up to a peak value.
- A further increase in ρ_{col} beyond this peak results in a reduction of the cell spread area (mean and standard deviation).
- The ρ_{col} at which the mean cell area reaches a peak decreases with decreasing E_{sub}.
- At a fixed ρ_{col}, the mean and standard deviation of the spread area increase with increasing E_{sub}.

The ρ_{col} directly influences the forces in adhesion complexes and, consequently, the adhesion free-energy. This, in turn, influences the spread states that cells assume in achieving homeostasis. A low ρ_{col} lowers the probability of a cell becoming highly spread, as sufficient complexes cannot form to support the tractions imposed by the substrate. Conversely, at a high ρ_{col} the cell may form more adhesion complexes, lowering the associated free-energy. Thus, the probability of cells having a high spread area increases. The influence of E_{sub} and ρ_{col} is highly coupled, as demonstrated in Figure 3 and 5. A deformable substrate lowers the probability of a cell becoming highly spread, reducing the cell tractions and thereby causing the peak mean spread area to occur at a lower ρ_{col}.

In statistical thermodynamics a closed system in a constant temperature and pressure environment attains equilibrium at minimum Gibbs free-energy. However, metabolic systems such as cells cannot be viewed in this manner; in fact, cells never attain an equilibrium minimum free-energy state while alive. The approach developed by Shishvan *et al.* (15) (extended in the current study) acknowledges this and predicts the statistics of biological observables (e.g. cell area, aspect ratio etc.) under the constraint that the cell maintains a homeostatic state. In previous studies, the importance of considering the system free-energy in the interpretation of cell spreading behaviour has been recognized (13, 29). McEvoy *et al.* (13) identified low (or minimum) free-energy cell spread states within a limited phase space of axisymmetric configurations. This simplified approach provided a reasonable approximation of the detailed trends computed in the current study (as observed experimentally (3)) which can be explained by the fact that low free-energy states will of course be highly probable within the *homeostatic ensemble*; see eq. (1). While McEvoy *et al.* (13) correctly demonstrate that cell spreading is governed by a competition between decreasing cytoskeletal and adhesion free-energy and increasing elastic energy, the identification of a low or minimum free-energy configuration is not physically appropriate for a fluctuating system. Therefore, the emergence of such an energetic competition within the statistical mechanics framework of the homeostatic ensemble provides a significant advance in current understanding of the influence of ligand density and substrate stiffness on cell spreading. Importantly, this framework correctly predicts the trends for observables such the spread area and spread shape as a function of environmental cues such as stiffness and ligand density, while also quantifying inherent statistical variability in these observations. The *homeostatic ensemble for cells*, expanded to include the focal adhesion formation and an associated adhesion free-energy contribution, provides new insight into observed cell behaviour on deformable collagen coated substrate. The model may readily be used to simulate more complex extra-cellular environments, including the spreading of cells on ligand patterned ridges and ligand patterned micro-pillars. Furthermore, the computational framework will be extended in a future study to explore the influence of gradients of ligand density on cell motility.

Acknowledgements

Funding support was provided by the Irish Research Council (IRC) postgraduate scholarship (GOIPG/2015/2954), the National University of Ireland Galway Hardiman scholarship, and the Science Foundation Ireland (SFI-12/IP/1723). The authors would like to acknowledge the Irish Centre for High-End Computing (ICHEC) for provision of computational facilities and support.

Author contributions

All authors contributed to the development and implementation of the computational model. EMcE performed all simulations and created all figures. EMcE, JPMcG and VSD analysed the results and wrote the article. JPMcG and VSD designed and coordinated the research.

References

1. Lange, L.A., D.W. Bowden, C.D. Langefeld, L.E. Wagenknecht, J.J. Carr, S.S. Rich, W.A. Riley, B.I. Freedman, B.A. Oostra, and C.M. van Duijn. 2002. Heritability of carotid artery intima-medial thickness in type 2 diabetes. Stroke. 33: 1876–81.

2. Chow, M.J., R. Turcotte, C.P. Lin, and Y. Zhang. 2014. Arterial extracellular matrix: A mechanobiological study of the contributions and interactions of elastin and collagen. Biophys. J. 106: 2684–2692.

3. Engler, A., M. Sheehan, H.L. Sweeney, and D.E. Discher. 2003. Substrate compliance vs ligand density in cell on gel responses. Eur. Cells Mater. 6: 7–8.

4. Jacot, J., A. McCulloch, and J. Omens. 2008. Substrate stiffness affects the functional maturation of neonatal rat ventricular myocytes. Biophys. J. 95: 3479–3487.

5. Arnold, M., E.A. Cavalcanti-Adam, R. Glass, J. Blümmel, W. Eck, M. Kantlehner, H. Kessler, and J.P. Spatz. 2004. Activation of Integrin Function by Nanopatterned Adhesive Interfaces. ChemPhysChem. 5: 383–388.

6. Ronan, W., V.S. Deshpande, R.M. McMeeking, and J.P. McGarry. 2014. Cellular contractility and substrate elasticity: A numerical investigation of the actin cytoskeleton and cell adhesion. Biomech. Model. Mechanobiol. 13: 417–435.

7. McGarry, J.P., J. Fu, M.T. Yang, C.S. Chen, R.M. McMeeking, A.G. Evans, and V.S. Deshpande. 2009. Simulation of the contractile response of cells on an array of micro-posts. Philos. Trans. A. Math. Phys. Eng. Sci. 367: 3477–3497.

8. Pirentis, A.P., E. Peruski, A.L. Iordan, and D. Stamenović. 2011. A Model for Stress Fiber Realignment Caused by Cytoskeletal Fluidization During Cyclic Stretching. Cell. Mol. Bioeng. 4: 67–80.

9. Vernerey, F.J., and M. Farsad. 2014. A mathematical model of the coupled mechanisms of cell adhesion, contraction and spreading. J. Math. Biol. 68: 989–1022.

10. Vernerey, F.J., and U. Akalp. 2016. Role of catch bonds in actomyosin mechanics and cell mechanosensitivity. Phys. Rev. E. 94: 012403.

11. Mogilner, A., and B. Rubinstein. 2005. The Physics of Filopodial Protrusion. Biophys. J. 89: 782–795.

12. Akalp, U., C. Schnatwinkel, M.P. Stoykovich, S.J. Bryant, and F.J. Vernerey. 2017. Structural Modeling of Mechanosensitivity in Non-Muscle Cells: Multiscale Approach to Understand Cell Sensing. ACS Biomater. Sci. Eng. 3: 2934–2942.

13. McEvoy, E., V.S. Deshpande, and P. McGarry. 2017. Free energy analysis of cell spreading. J. Mech. Behav. Biomed. Mater. 74: 283–295.

14. Théry, M., A. Pépin, E. Dressaire, Y. Chen, and M. Bornens. 2006. Cell distribution of stress fibres in response to the geometry of the adhesive environment. Cell Motil. Cytoskeleton. 63: 341–355.

15. Shishvan, S.S., A. Vigliotti, and V.S. Deshpande. 2018. The homeostatic ensemble for cells. Biomech. Model. Mechanobiol. : 1–32. https://doi.org/10.1007/s10237-018-1048-1

16. Jaynes, E.T. 1957. Information Theory and Statistical Mechanics. Phys. Rev. 106: 620–630.

17. Vigliotti, A., W. Ronan, F.P.T. Baaijens, and V.S. Deshpande. 2016. A thermodynamically motivated model for stress-fiber reorganization. Biomech. Model. Mechanobiol. 15: 761–789.

18. Weafer, P.P., W. Ronan, S.P. Jarvis, and J.P. McGarry. 2013. Experimental and Computational Investigation of the Role of Stress Fiber Contractility in the Resistance of Osteoblasts to Compression. Bull. Math. Biol. 75: 1284–1303.

19. Reynolds, N.H., W. Ronan, E.P. Dowling, P. Owens, R.M. McMeeking, and J.P. McGarry. 2014. On the role of the actin cytoskeleton and nucleus in the biomechanical response of spread cells. Biomaterials. 35: 4015–4025.

20. Dowling, E.P., W. Ronan, G. Ofek, V.S. Deshpande, R.M. McMeeking, K. a Athanasiou, and J.P. McGarry. 2012. The effect of remodelling and contractility of the actin cytoskeleton on the shear resistance of single cells: a computational and experimental investigation. J. R. Soc. Interface. 9: 3469–79.

21. Dowling, E.P., and J.P. McGarry. 2014. Influence of Spreading and Contractility on Cell Detachment. Ann. Biomed. Eng. 42: 1037–1048.

22. McGarry, J.P., and P.E. McHugh. 2008. Modelling of in vitro chondrocyte detachment. J. Mech. Phys. Solids. 56: 1554–1565.

23. Selhuber-Unkel, C., T. Erdmann, M. López-García, H. Kessler, U.S. Schwarz, and J.P. Spatz. 2010. Cell Adhesion Strength Is Controlled by Intermolecular Spacing of Adhesion Receptors. Biophys. J. 98: 543–551.

24. Gaudet, C., W. a Marganski, S. Kim, C.T. Brown, V. Gunderia, M. Dembo, and J.Y. Wong. 2003. Influence of type I collagen surface density on fibroblast spreading, motility, and contractility. Biophys. J. 85: 3329–3335.

25. Ren, K., L. Fourel, C.G. Rouvière, C. Albiges-Rizo, and C. Picart. 2010. Manipulation of the adhesive behaviour of skeletal muscle cells on soft and stiff polyelectrolyte multilayers. Acta Biomater. 6: 4238–4248.

26. Prager-Khoutorsky, M., A. Lichtenstein, R. Krishnan, K. Rajendran, A. Mayo, Z. Kam, B. Geiger, and A.D. Bershadsky. 2011. Fibroblast polarization is a matrix-rigidity-dependent process controlled by focal adhesion mechanosensing. Nat. Cell Biol. 13: 1457–1465.

27. Deroanne, C., C.M. Lapiere, and B. V. Nusgens. 2001. In vitro tubulogenesis of endothelial cells by relaxation of the coupling extracellular matrix-cytoskeleton. Cardiovasc. Res. 49: 647–658.

28. Pelham, R.J., and Y.-L. Wang. Cell Locomotion and Focal Adhesions are Regulated by Substrate Flexibility. Proc. Natl. Acad. Sci. U. S. A. 94: 13661–1366.

29. Shenoy, V.B., H. Wang, and X. Wang. 2016. A chemo-mechanical free-energy-based approach to model durotaxis and extracellular stiffness-dependent contraction and polarization of cells. Interface Focus. 6: 20150067.

Figure captions

Figure 1: (a) Contours of bound stress-fibre protein concentrations $\widehat{N}_{\mathrm{b}}$ (green) with dominant alignment, focal adhesion distributions $\hat{C}$ (red), and overlays in commonly observed cell shapes at a given surface collagen density ρ_{col}. The substrate is rigid, and nucleus is highlighted in blue. The cell spread states for a given ρ_{col} have the same free-energy. Scale bar indicates undeformed cell radius R_0. Probability density functions for cells spread on a rigid substrate for 3 collagen densities, of (b) cell spread area ($\hat{A} = A/\pi R_0^2$), and (c) cell aspect ratio.

Figure 2: (a) Contours of bound stress-fibre protein concentrations $\widehat{N}_{\mathrm{b}}$ (green) with dominant alignment, focal adhesion distributions $\hat{C}$ (red), and overlays in commonly observed cell shapes at a given substrate stiffness E_{sub}. The surface collagen density ρ_{col} is fixed at 33 ng cm^{-2}, and the nucleus is highlighted in blue. The cell spread states for a given E_{sub} have the same free-energy. Scale bar indicates undeformed cell radius R_0. Probability density functions for cells spread on substrates of different stiffness at a surface collagen density ρ_{col} of 33 ng cm^{-2}, of (b) cell spread area ($\hat{A} = A/\pi R_0^2$), and (c) cell aspect ratio.

Figure 3: Contour plots for predicted mean spread area (a) and mean cell aspect ratio (b) in the $\rho_{\mathrm{col}} - E_{\mathrm{sub}}$ space. (c) Predicted cell area (mean$\pm$SD) and (d) cell aspect ratio (mean$\pm$SD) as a function of surface collagen density ρ_{col} for cells spread on substrates of different stiffness (red-rigid, yellow-32kPa, green-8kPa). Sample cell spread states are shown for a given substrate in (a, b).

Figure 4: Probability density functions for cells spread on a rigid substrate for 3 surface collagen densities ρ_{col}, of (a) Gibbs free-energy, (b) adhesion free-energy, (c) cytoskeletal free-energy, and (d) elastic free-energy ($\hat{F}_{elas} = \hat{F}_{passive} + \hat{F}_{sub}$).

Figure 5: Predicted adhesion (a-c), cytoskeletal (d-f), elastic (g-i), and substrate (j-l) free-energy (mean$\pm$SD) as a function of surface collagen density ρ_{col} for cells spread on rigid, stiff, and compliant substrates.

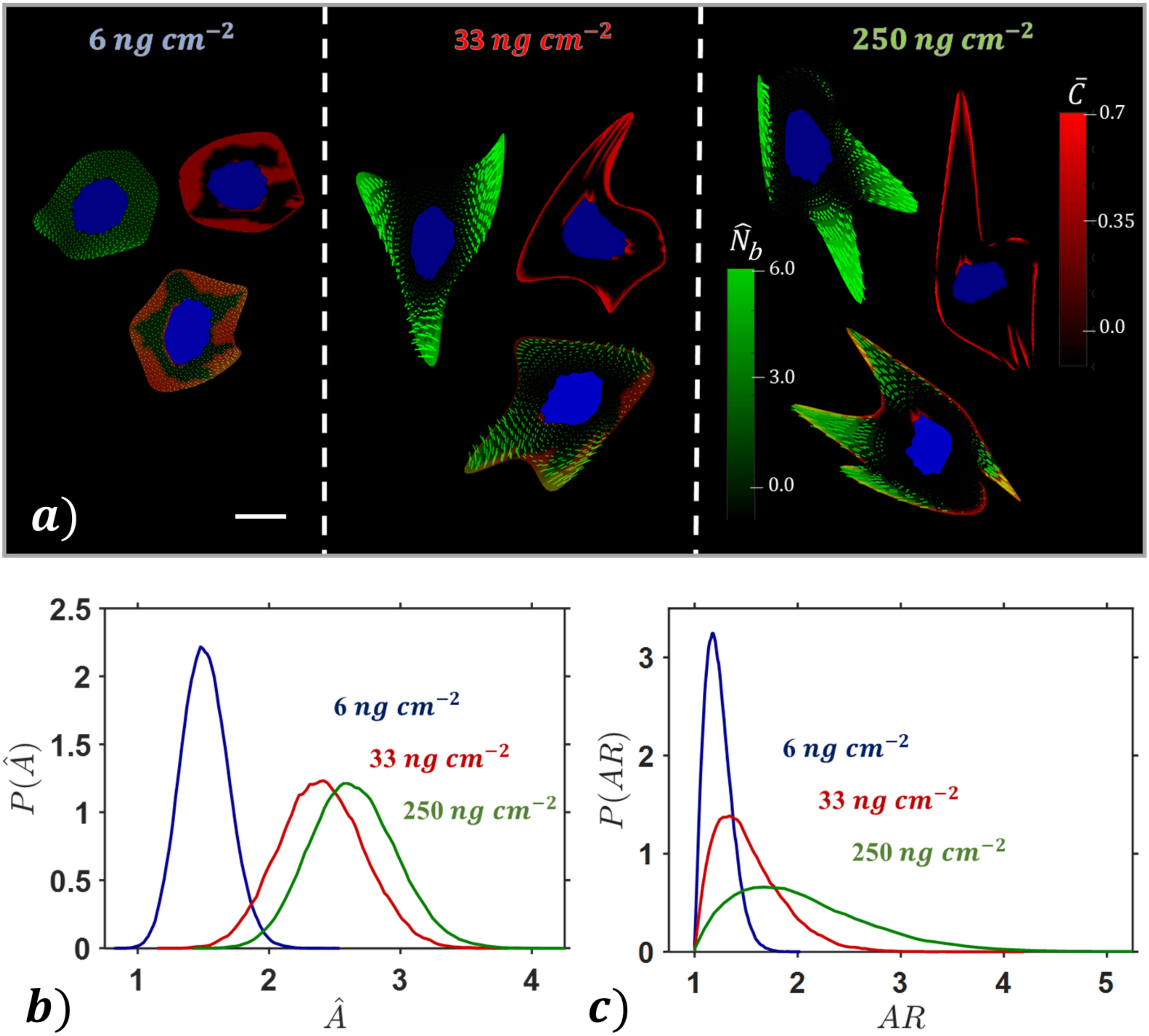
a)
6 ng cm^-2
33 ng cm^-2
250 ng cm^-2
$\hat{N}_b$
6.0
3.0
0.0
$\bar{C}$
0.7
0.35
0.0
b)
$P(\hat{A})$
$\hat{A}$
2.5
2
1.5
1
0.5
0
1
2
3
4
6 ng cm^-2
33 ng cm^-2
250 ng cm^-2
c)
$P(AR)$
AR
3
2
1
0
1
2
3
4
5
6 ng cm^-2
33 ng cm^-2
250 ng cm^-2

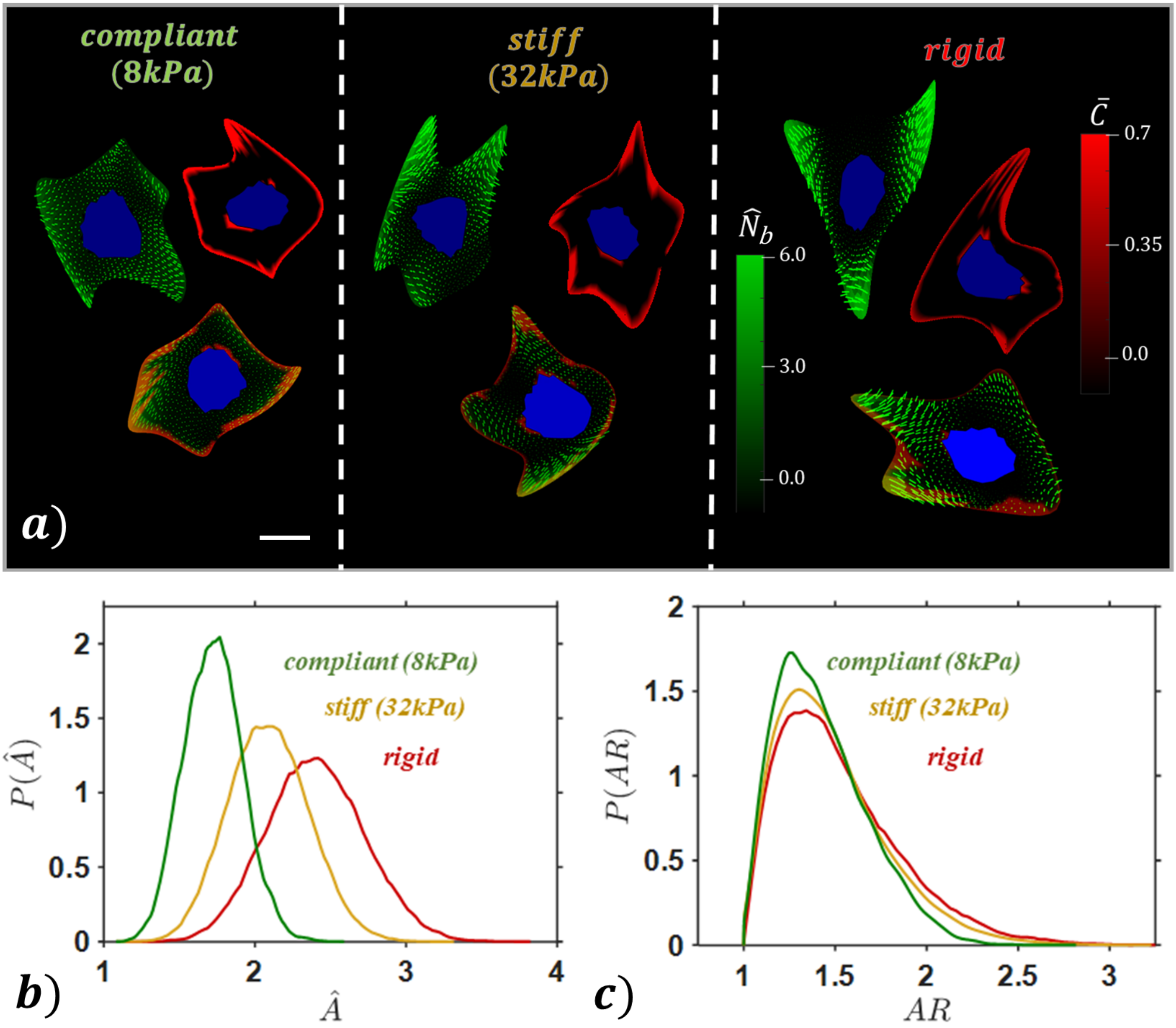

compliant (8kPa)
stiff (32kPa)
rigid
$\bar{C}$
0.7
0.35
0.0
$\hat{N}_b$
6.0
3.0
0.0
a)
$P(\hat{A})$
$\hat{A}$
0
0.5
1
1.5
2
1
2
3
4
compliant (8kPa)
stiff (32kPa)
rigid
b)
$P(AR)$
AR
0
0.5
1
1.5
2
1
1.5
2
2.5
3
compliant (8kPa)
stiff (32kPa)
rigid
c)

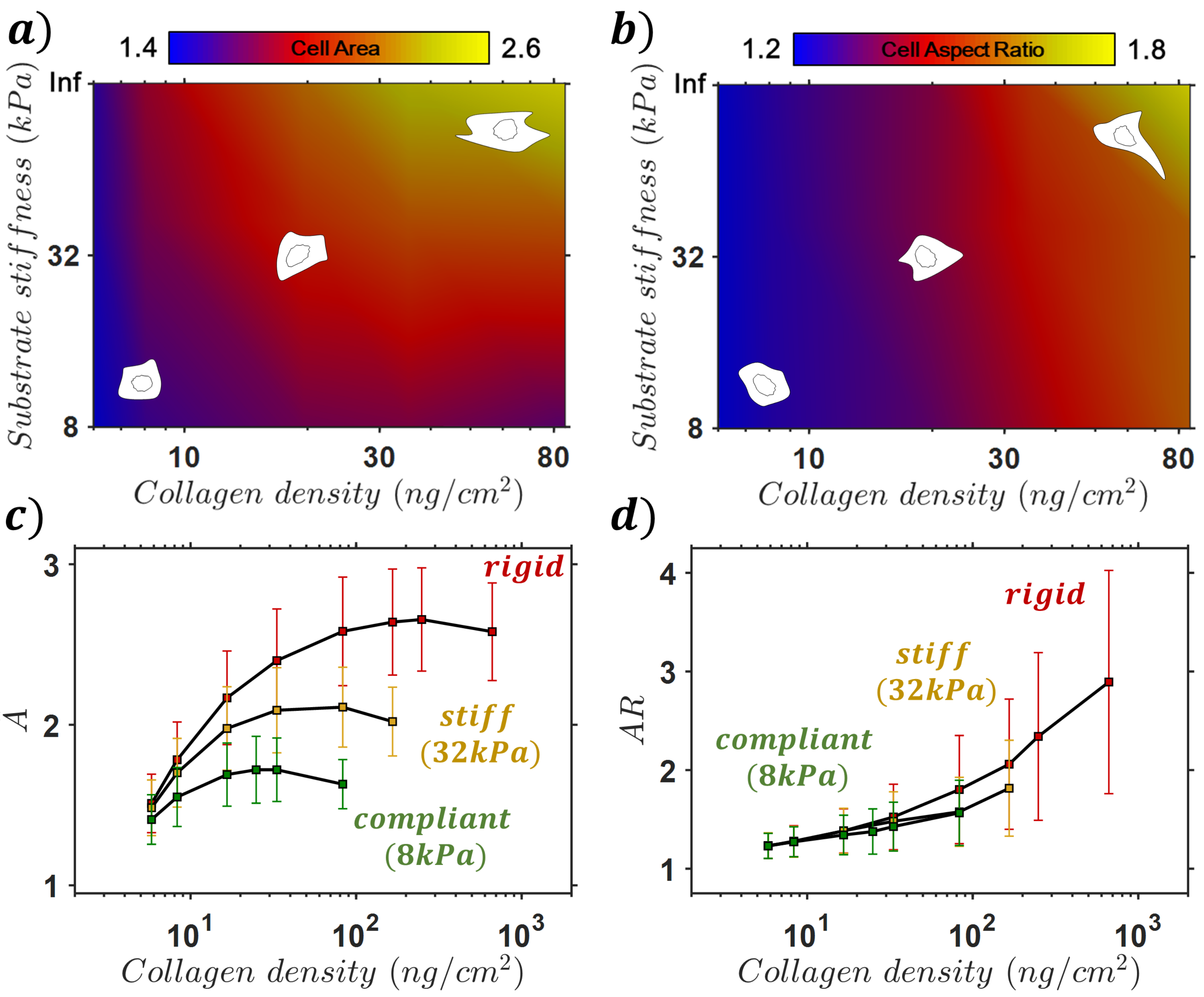
a)
1.4
Cell Area
2.6
Inf
32
8
10
30
80
Substrate stiffness (kPa)
Collagen density (ng/cm²)
b)
1.2
Cell Aspect Ratio
1.8
Inf
32
8
10
30
80
Substrate stiffness (kPa)
Collagen density (ng/cm²)
c)
3
2
1
Â
rigid
stiff
(32kPa)
compliant
(8kPa)
10¹
10²
10³
Collagen density (ng/cm²)
d)
4
3
2
1
AR
rigid
stiff
(32kPa)
compliant
(8kPa)
10¹
10²
10³
Collagen density (ng/cm²)

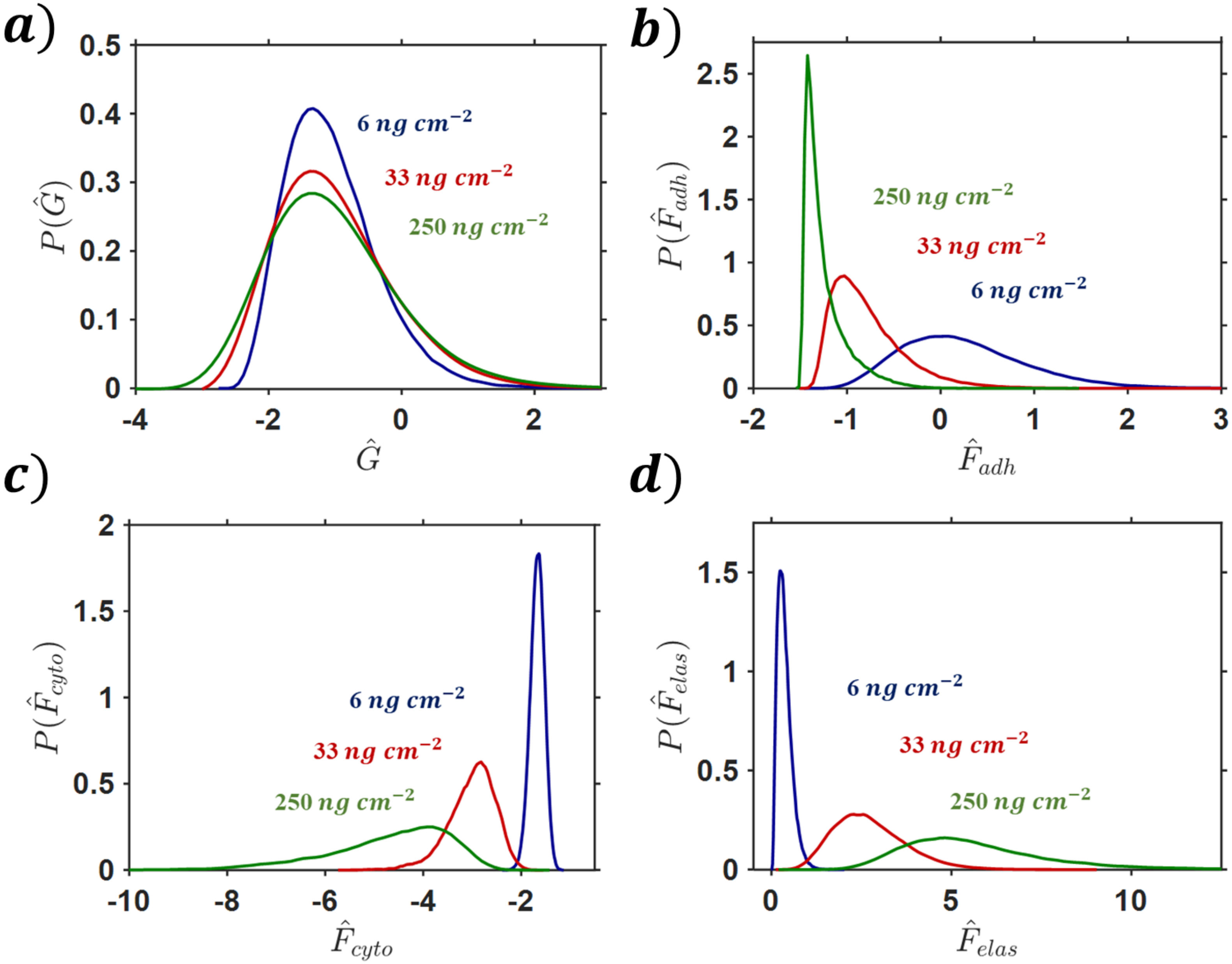
a)
b)
c)
d)
$P(\hat{G})$
$\hat{G}$
6 ng cm^{-2}
33 ng cm^{-2}
250 ng cm^{-2}
0.5
0.4
0.3
0.2
0.1
0
-4
-2
0
2
$P(\hat{F}_{adh})$
$\hat{F}_{adh}$
2.5
2
1.5
1
0.5
-1
3
$P(\hat{F}_{cyto})$
$\hat{F}_{cyto}$
-10
-8
-6
$P(\hat{F}_{elas})$
$\hat{F}_{elas}$
5
10

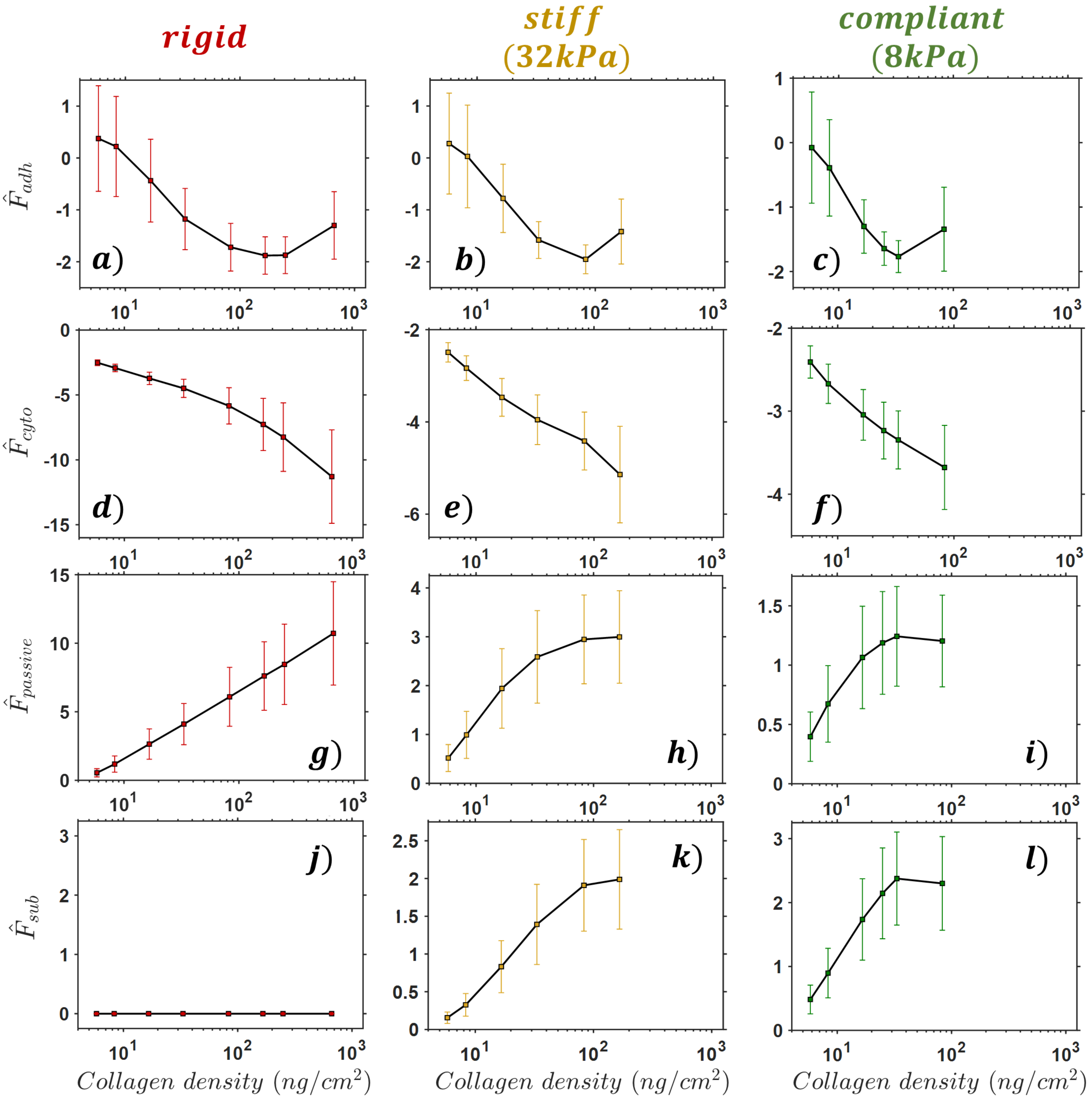
rigid
stiff (32kPa)
compliant (8kPa)
$\hat{F}_{adh}$
$\hat{F}_{cyto}$
$\hat{F}_{passive}$
$\hat{F}_{sub}$
a)
b)
c)
d)
e)
f)
g)
h)
i)
j)
k)
l)
10^1
10^2
10^3
Collagen density (ng/cm^2)
Collagen density (ng/cm^2)
Collagen density (ng/cm^2)